Geoacoustic characterization by the image source method: a sensitivity study

S. Pinson[a], L. Guillon[a] and P. Cervenka[b]

[a]IRENav, BCRM Brest, Ecole Navale, CC 600, 29240 Brest Cedex9, France
[b]CNRS UMR 7190, UPMC (P6) Institut Jean le Rond d'Alembert, 2, place de la gare de ceinture, 78210 Saint-Cyr-L'Ecole, France
samuelpinson@yahoo.fr

A new method for measuring the sound speed profile of the seafloor has been recently proposed (JASA, vol. 128, pp. 1685-1693): the image source method. This method is based on a physical model of the acoustic field generated by a point source and reflected by a layered media. Under the Born approximation, the reflected signal can be modeled as a sum of contributions coming from image sources relative to the seabed layers. Consequently, the seabed geometry and sound speed profile can be recovered by exploiting the localization of these images. We present here a study about the sensitivity with the relative noise level in the localization of the image sources.

1 Introduction

Most of the present techniques to characterize the seafloor in shallow water by acoustics are based on inversion process such as, for example, matched field methods [1]. In reference [7] and [8] a new method based on the detection of image sources is described. The configuration is a broadband source and a vertical or an horizontal array. The method considers geological interfaces as acoustical mirrors on which images of the real source appear. The advantage of imaging the seafloor by searching for point sources is that it becomes possible to use array processing to detect the sources and then use the position of these image sources to determine the seabed structure without inversion process. But, "The inversion would be incomplete if not followed by an analysis of the uncertainties of the result"[4]. In [7], a range dependent seafloor sound speed characterization is presented and a standard deviation of the sound speed structure is proposed by using the redundancy of information. In this paper, we focus the uncertainty study on the noise effects on the sound speed profile (SSP) calculation.

The image source method principles are recalled in section 2 and the data used are presented in section 3. SSP uncertainties due to the noise are then studied in section 4 and computed for simulated and real data.

2 The image source method

2.1 Principle

The image source method is based on the ray theory and the Born approximation [8]. To model the reflection of an emitted wave as a collection of image sources, the following points are assumed. First, the water column and the geologic layers are homogeneous, the latter being all horizontal. Second, the angle of incidence at an interface is smaller than the critical angle. Third, only the first reflections are taken into account (Born approximation); multiple reflections between interfaces are considered too low in amplitude to interfere with the first ones and be detectable. In this case, each reflection on an interface (Fig. 1a) is identified by the receiver as a wave coming from an image source which can be described in an equivalent system: the structure (water + sediment layers) above this interface and its symmetric structure. So, each image is represented in a different equivalent system but, for any given system, the places of the components (water and layer and their symmetric structure) have no consequences on the angle of arrival or on the total travel time. Considering only these parameters, it is then possible to merge all the equivalent systems in a single one which contains all the image sources (Fig. 1b). In this system, all the thicknesses are doubled and the images are located on the interfaces and at a zero horizontal offset relative to the source.

The recorded signals from an array of hydrophones are used to produce a map of the image sources. If the layer
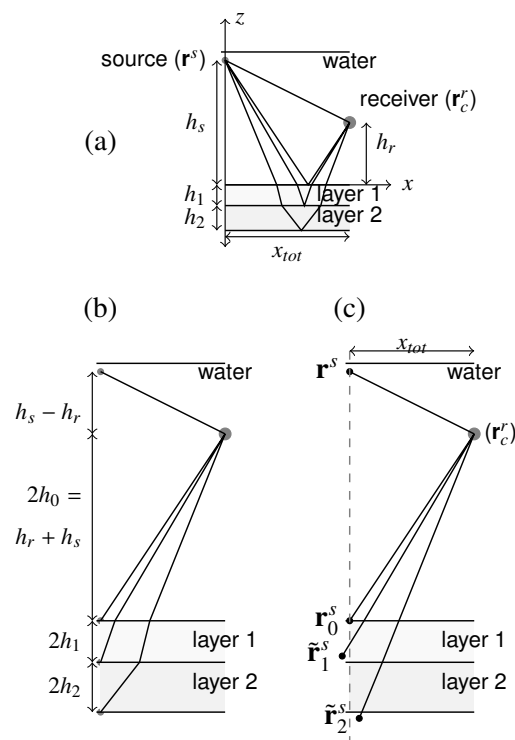

Figure 1: Modeling of the seafloor with image sources: (a) original configuration, (b) the equivalent system. (c) Image sources not aligned on the vertical source axis due to the water sound-speed everywhere assumption.

thicknesses and sound speeds are known, the image sources are located on the vertical source axis because of refraction (Fig. 1b). But if this is not the case, the map is produced with a constant water sound speed everywhere which leads to a wrong position of the image sources (Fig. 1c). Even if their locations are wrong, two parameters are correct:

- the arrival angles of the waves from the images on the sensor,

- the travel times of the waves from the images to the sensor.

The image source method principle is to use this parameters to obtain the layer thicknesses and sound speeds.

2.2 Algorithm

The algorithm is recursive. The starting parameters are the heights of source h_s and receiver h_r, the range x_{tot} and the water sound speed c_0. Image source coordinates $\mathbf{r}_i^s$ are numbered from $i = 0$, and the real source coordinate $\mathbf{r}^s$ has no index. The first image source coordinate $\mathbf{r}_0^s$ corresponding to the first reflection on the water bottom is correct. Then using the second image coordinate $\mathbf{r}_1^s$, the first layer thickness

and sound-speed can be calculated. This process is repeated for the next layers.

Supposing that the sound speeds (c_0, c_1, ..., c_{l-1}) and thicknesses (h_0, h_1, ..., h_{l-1}) of the layers 0 to $l-1$ are known, the coordinate $\mathbf{r}_l^s$ gives the information to get the layer l parameters. The coordinate $\mathbf{r}_l^s$ of the image source l located in a water sound-speed medium gives a couple of parameters ($t_{tot}^{(l)}$, $\theta_0^{(l)}$) characterizing the ray between the image source and the receiver: $t_{tot}^{(l)} = \left| \mathbf{r}_c^r - \mathbf{r}_l^s \right| / c_0$ is the travel time, $\mathbf{r}_c^r$ is the sensor coordinate and $\theta_0^{(l)}$ is the angle of arrival of the ray on the sensor (Fig. 2). By convention, the sum of h_r (height of the receiver) and h_s (height of the source) is called $2h_0$.
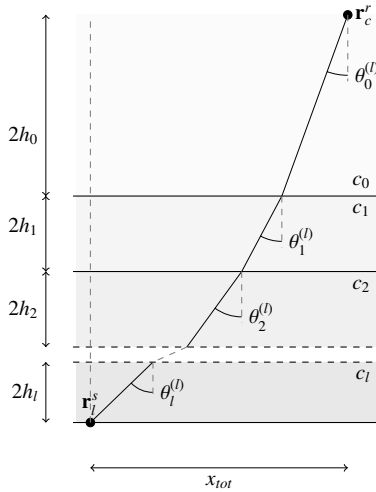

Figure 2: Refracted ray in a medium with known layer sound speeds and thicknesses.

The sound speed in layer l is computed by [7]:

$$c_l^2 = \frac{c_0}{t_l^{(l)} \sin \theta_0} \left(x_{tot} - \sum_{p=0}^{l-1} 2h_p \tan \theta_p^{(l)} \right), \qquad (1)$$

with:

$$\theta_{0<i<l-1}^{(l)} = \sin^{-1} \left(\frac{c_i}{c_0} \sin \theta_0^{(l)} \right), \qquad (2)$$

where $\theta_p^{(l)}$ is the incidence angle in the layer p of the ray between $\mathbf{r}_l^s$ and $\mathbf{r}_c^r$.
Once the sound-speed is computed, the incidence angle in layer l is obtained by the Snell-Descartes law and the thickness of the layer l is obtained by:

$$h_l = \frac{1}{2} c_l t_l^{(l)} \cos \theta_l^{(l)} = \frac{1}{2 \tan \theta_l^{(l)}} \left(x_{tot} - \sum_{p=0}^{l-1} 2h_p \tan \theta_p^{(l)} \right). \quad (3)$$

The equations are the same than those obtained by Bryan [3]. However, Bryan's method needs an horizontal array of sensors which is not a limitation of the image source method [8].

3 Data

3.1 Data from SCARAB experiment

Real data has been acquired in June 1998 near Elba Island in Italy as part of the SCARAB (Scattering And ReverberAtion from the sea Bottom) experiment series (see Ref. [5] for

details). The configuration is a broadband source (100 Hz - 6 kHz or $\approx$ 1ms duration), 20 cm bellow the sea surface, and an array made of 15 hydrophones irregularly spaced over 64 m. The lowermost hydrophone is around 12 m above the seafloor (Fig. 3). One of the recorded signals is shown in Figure 4. One can note the presence of a non-negligible additive noise but numerous seabed reflections are nevertheless still visible. The physical phenomenon that leads to recovery of the SSP is the refraction of sound waves in the layers. Then, it implies that larger the range between source and receivers, higher the refraction phenomenon. But the range also needs to be short enough to avoid a total reflection phenomenon on the interfaces which occurs at high incident angles. A 45° incident angle on the seafloor for the middle of the array is far from the critical angle and is a good compromise. So, with a 150 m water depth, the range between source and receivers is 200 m.
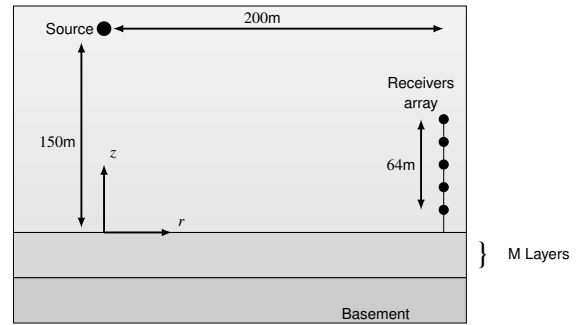

Figure 3: Sketch of the experiment. The source is 200 m away from the vertical array. The receiver array, moored on the seafloor, is made of 15 hydrophones, is 64 m long. The lowermost hydrophone is around 12 m above the seafloor.
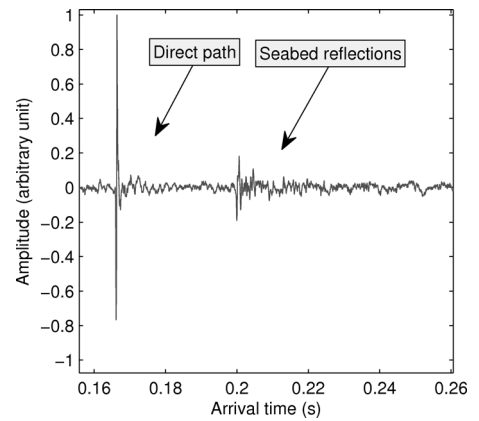

Figure 4: Temporal signal recorded at the 8th hydrophone of the array.

3.2 Synthetic data

For modeled data, the configuration is the same as for experimental data. Synthetic data is obtained by a numerical evaluation of the Sommerfeld integral, the exact analytical solution of the reflection of a spherical wave on layered media [2]. The geoacoustic structure for the synthetic data is chosen simple enough to avoid difficult interpretation. The simulated seabed is composed of 9 fluid sediment layers covering a semi-infinite fluid basement (Tab. 1). The temporal signal simulated for the 8th hydrophone of the

array (Fig. 5) shows visible echoes from the 10 interfaces. Echoes from these interfaces are identified on Figure 5. Multiple reflections between interfaces are present in the computed signal but these echoes amplitudes are too small to be visible or to interfere with echoes from direct reflections.

Layer	Sound speed (m/s)	Density	Thickness (m)
Water	1500	1	.
1	1520	1.1	3
2	1540	1.2	3.5
3	1600	1.5	4
4	1630	1.7	2
5	1700	1.9	6
6	1720	2	2
7	1800	2.5	5
8	1900	3	3
9	1920	3.1	2
Basement	2000	3.6	.

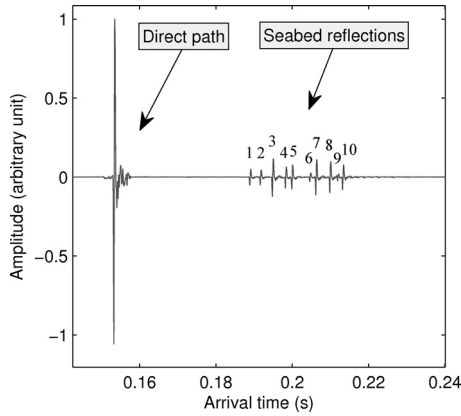Table 1: Geoacoustic parameters for the synthetic data. The media used here are non-dissipative.

Figure 5: Temporal signal computed for the 8th hydrophone of the array. Numbers 1-10 stand for interface reflections.

4 Noise uncertainties

In the SSP recovering process, there is many error sources. Errors can come from measurement itself (transducer coordinates, knowledge of the emitted pulse,...), the image source method hypothesis (Born approximation, spherical geometrical spreading approximation,...), the geological hypothesis (interface roughnesses, volumetric inhomogeneities, interface dip angles,...) or from the noise influence on image source localization. In this paper, the study is focused on the noise effects.

4.1 Noise influence on image sources localization

The image sources are located with array processing technics. The localization accuracy depends on 4 factors: the beam width of the array, the emitted pulse duration, the image source sound level and the noise level. To analyze the noise influence on the angular localization, we consider a linear array directivity function [6]:

$$\mathcal{D}(\psi) = \frac{\sin\left(\pi \frac{L \sin \psi}{\lambda}\right)}{\pi \frac{L \sin \psi}{\lambda}} \approx \frac{\sin\left(\pi \frac{L \psi}{\lambda}\right)}{\pi \frac{L \psi}{\lambda}}, \qquad (4)$$

where λ is the wavelength, L is the array aperture and ψ is the angle of arrival ($\psi = 0$ in front of the array). The approximation is valid in the main lobe if the directivity is accurate enough.

Considering the signal intensity I_s and the noise intensity I_b, the localization of the maximum of $\mathcal{D}(\psi)$ is subject to an uncertainty $\delta\psi$ due to the noise. To characterize this uncertainty, we search $\delta\psi$ such that the noise intensity implies an error on the localization of the maximum:

$$I_s \mathcal{D}^2(\delta\psi) + I_b = I_s . \qquad (5)$$

Using the second order expansion of the sinc function, equation (5) becomes:

$$1 - \frac{\pi^2}{6}\left(\frac{L\delta\psi}{\lambda}\right)^2 = \sqrt{\frac{I_s - I_b}{I_s}} . \qquad (6)$$

If $I_b \ll I_s$, the uncertainty $\delta\psi$ is obtained by:

$$\delta\psi \approx \frac{\lambda \sqrt{3}}{\pi L}\sqrt{\frac{I_b}{I_s}} = \frac{\lambda \sqrt{3}}{\pi L} 10^{\frac{-SNR}{20}}, \qquad (7)$$

where $\text{SNR} = 10\log_{10}(I_s/I_b)$ is the signal to noise ratio in dB.

The method is the same to analyze the image source range localization. The image source range resolution is given by the pulse duration. Considering that the pulse envelope $\left|f^{\mathcal{H}}(t)\right|$ is a Gaussian function, the range localization uncertainty δd is given such that the noise intensity implies an error on the localization of the maximum:

$$I_s \left|f^{\mathcal{H}}(\delta d/c_0)\right|^2 + I_b = I_s , \qquad (8)$$

where $\left|f^{\mathcal{H}}(t)\right| = e^{-\frac{t^2}{2\sigma^2}}$ with $2\sigma = 1$ ms (the pulse duration).

Using the expansion $\ln(1 - I_b/I_s) \approx -I_b/I_s$ for $I_b/I_s \ll 1$, equation (8) becomes:

$$\delta d = \sqrt{-c_0^2 \sigma^2 \ln(1 - I_b/I_s)} \approx c_0 \sigma \sqrt{\frac{I_b}{I_s}}, \qquad (9)$$

or:

$$\delta d \approx c_0 \sigma 10^{-\frac{SNR}{20}} . \qquad (10)$$

4.2 Example with simulated data

To study the noise influence on the computed SSP, numerical simulations are done with 3 different noise levels. The rms source level is 207 dB re 1μPa @ 1 m (the same as in the SCARAB experiment). The noise spectrum densities are 70, 80 and 90 dB re 1μPa / $\sqrt{\text{Hz}}$. The signal bandwidth being 6 kHz, this different noise spectrum densities correspond to a noise level of 108, 118 and 128 dB re 1μPa (Fig. 6a, 6b and 6c). The geometrical spreading losses are between -51 and -48.5 dB (as a function of the hydrophone or image source considered). The rms image source levels are between -27 and -16 dB lower than the real source level. So the echo signal to noise ratios are between 1 and 14.5 dB for the highest noise (128 dB re 1μPa, Fig. 6c). For each noise level, 20 inversions are realized with different noise realizations (Fig. 6d, 6e and 6f). One can see a sensitivity of the SSP to the noise level.

From theorical image source locations and amplitudes, the uncertainties $\pm\delta d$ and $\pm\delta\theta$ (Equations (10) and (7)) are computed as a function of the noise level. Then a minimum and a maximum layer sound speed are computed supposing that upper layer sound speeds are correct. In fact, when an error is made on a layer sound speed, numerical experiments show that the error seems to be compensated by the next layer sound speed [7]. Theoritical uncertainties obtained with the 108 dB *re* 1μPa and 118 dB *re* 1μPa noise level (Fig 6g and 6h) correspond correctly enough to the sound speed distributions of the different noise realization (Fig. 6d and 6e). On the other hand, the theoritical uncertainties obtained with the 128 dB *re* 1μPa noise level (Fig. 6i) are much higher than the sound speed distributions of the different noise realization (Fig. 6f). This overestimation comes from the good signal to noise ratio hypothesis to obtain the equations (10) and (7) that is not valid in this case.

4.3 Example with SCARAB data

The real data noise level is estimated on the part of the recorded signal before the direct path between the source and the hydrophone. Echo levels are estimated by analyzing the detected image source amplitudes. Thus, uncertainties $\pm\delta d$ and $\pm\delta\theta$ can be estimated. Then, a minimum and a maximum layer sound speed are computed supposing that upper layer sound speeds are correct (Fig. 7). Ground truth from SCARAB experiment [5] has been obtained for the 6 first meters which is not enough to compare with the SSP obtained with the image source method. So the result is compared with that of Holland and Osler. Many layers detected with Holland and Osler method are not detected with the image source method but the global shape of the SSP are in a good agreement. One can see that the effect of the uncertainties on thin layers is very important even if their corresponding echoes have a good signal to noise ratio (the first echoes from the top layers are higher in amplitude than the deeper ones). So the uncertainty on a layer sound speed depends on both the image location uncertainty and the layer thickness.
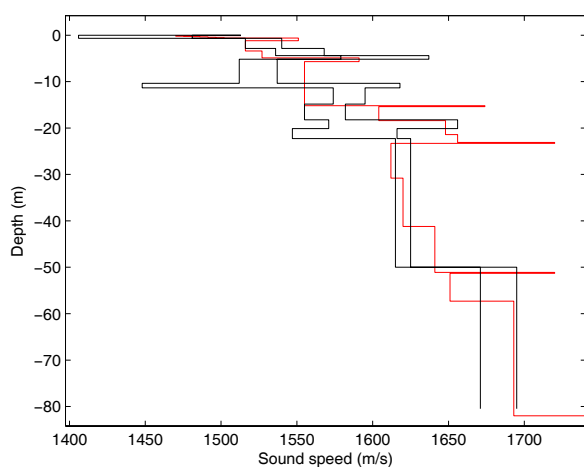

Figure 7: Black: minimum and maximum SSP using the uncertainties $\pm\delta d$ and $\pm\delta\theta$. Red: Holland and Osler result [5].

5 Conclusion

The main advantage of inverse methods in comparison with seismic method is that it is possible to estimate uncertainties in the result. Because of the angle of arrival and time of flight analysis to obtain the SSP, the image source method is close to seismic method. But this method enable the possibility to obtain uncertainties on its result. In this paper, a layer sound speed uncertainty is computed assuming that the upper layer sound speeds are correct. In fact, these upper layer errors should be taken into account. To study the influence of the upper layer errors, a theoretical study on the error propagation from a layer to another has to be performed. This is the object of a future work.

Acknowledgments

References

[1] AB Baggeroer, WA Kuperman, and PN Mikhalevsky. An overview of matched field methods in ocean acoustics. *IEEE Journal of Oceanic Engineering*, 18(4):401–424, 1993.

[2] L. Brekhovskikh and Y. Lysanov. *Fundamentals of Ocean Acoustics*. Springer-Verlag, Berlin, 1991.

[3] G.M. Bryan. The hydrophone–pinger experiment. *J. Acous. Soc. Am.*, 68:1403–1408, 1980.

[4] P. Gerstoft. Inversion of seismoacoustic data using genetic algorithms and a posteriori probability distributions. *Journal of the Acoustical Society of America*, 95(2):770–782, 1994.

[5] C.W. Holland and J. Osler. High resolution geoacoustic inversion in shallow water: A joint time and frequency domain technique. *J. Acoust. Soc. Am.*, 107:1263–1279, 2000.

[6] P.S. Naidu. *Sensor array signal processing*. CRC, 2001.

[7] S. Pinson. *Caractérisation des fonds marins par la méthode des sources images*. PhD thesis, Université de Bretagne Occidentale, 2011.

[8] S. Pinson and L. Guillon. Sound speed profile characterization by the image source method. *J. Acoust. Soc. Am.*, 128:1685–1693, 2010.
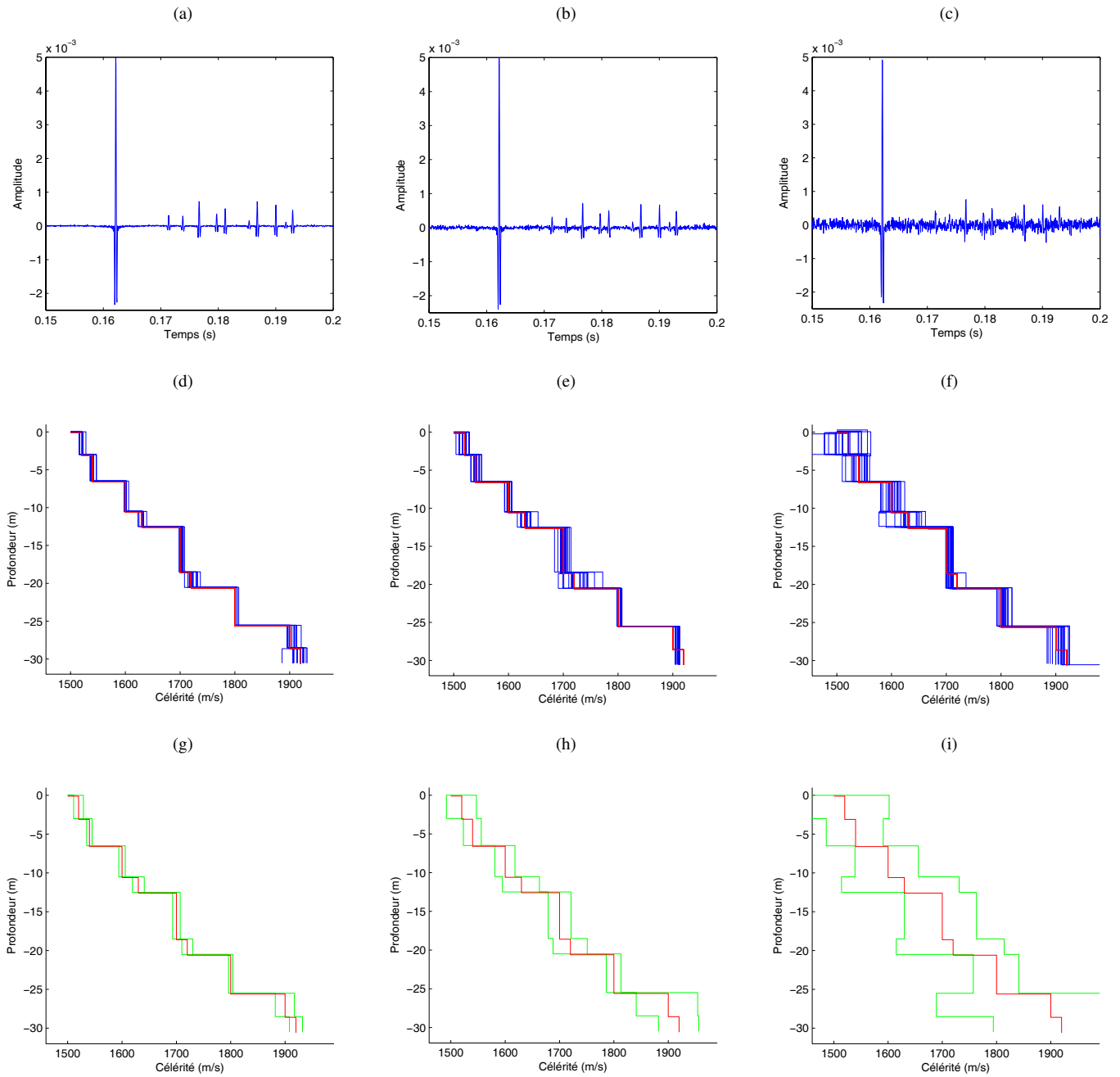
Figure 6: (a),(b),(c): Simulated signals for the first hydrophone with a 207 dB *re* 1μPa @ 1 m source level and different noise level ((a):108 dB *re* 1μPa, (b):118 dB *re* 1μPa, (c):128 dB *re* 1μPa).
(d),(e),(f): (Red) SSP of the model, (Blue) 20 computed SSP with different noise realizations for each moise level ((d):108 dB *re* 1μPa, (e):118 dB *re* 1μPa, (f):128 dB *re* 1μPa).
(g),(h),(i): (Red) SSP of the model, (Green) minimum and maximum SSP computed considering the image source location uncertainties $\pm\delta d$ and $\pm\delta\theta$ (Equations (10) and (7)) for each noise level ((g):108 dB *re* 1μPa, (h):118 dB *re* 1μPa, (i):128 dB *re* 1μPa).